RSC Advances

PAPER

View Article Online
View Journal | View Issue

Cite this: *RSC Adv.*, 2024, **14**, 21075

Deciphering the influence of Pd^{II} and Pd^{IV} oxidation states on non-standard chemical bonds within bis(jN-heterocyclic carbene) complexes: insights from DFT†

Jean Ongagna Moto, *[a] Abel Idrice Adjieufack, *[b] Simon Claude Ndika Ngomb,[a] Gaël Mouzong D'ambassa,[a] Suzane Leonie Djendo Mazia[a] and Désiré Mama Bikele*[a]

Received 27th May 2024
Accepted 18th June 2024

DOI: 10.1039/d4ra03893b

rsc.li/rsc-advances

Bis-N-heterocyclic carbene ligands (bis(NHC)) have introduced a new approach to designing homogeneous and heterogeneous catalysts, demonstrating the versatility of ligand concepts in catalysis. This study presents a computational analysis of palladium (+II and +IV) complexes containing either a normally (bis(nNHC)) or an abnormally (bis(aNHC)) bound CH_2-bridged bis-N-heterocyclic carbene ligand; in addition, ancillary ligands are permuted from chlorides (X = Cl) to bromides (X = Br). Density functional theory at the B3PW91/6-31G(d)/Lanl2DZ level in the gas phase was used to investigate the electronic structure and bonding properties of bis(NHC)$Pd^{II}X_2$ and bis(NHC)$Pd^{IV}X_4$ for bis(NHC) palladium(II) dihalide and palladium(IV) tetrachloride complexes, respectively. Results indicate that all of the palladium complex structures prefer a flexible boat-type conformation with an average C_{2v} symmetry, according to bond property ($C_{carbene}$–Pd and Pd–Cl[Br]) analysis. The strength of these bonds depends on coordinating halide ions (Cl^- and Br^-), the type of ligand (bis(nNHC) and bis(aNHC)), and the palladium oxidation state (+II and +IV). Analysis of thermodynamic parameters (ΔH^0, ΔG^0, and ΔE_{bind}) shows an increase in values from an abnormal to normal chelating mode in tetrahalides, whereas the opposite is observed for dihalide complexes. The lower π-backbonding ability of the metal, which is influenced by the quantity and size of halide ions involved, could be one possible explanation for this deficiency.

1 Introduction

Petroleum feedstocks (oil and gas), estimated at 100 000 and 300 000 barrels per year, currently represent the main source of fuel, chemicals, and materials in the world, although the exploitation and valorization of biomass (renewable source) are in full expansion.[1] Despite the fact that this resource is expected to be exploited for 50 years,[2] research on alternative uses of natural gas is aimed at limiting some of its effects and the gas emissions resulting from its use on the environment. Methane (60%), one of the main components of natural gas, is the main target because of its greater warming potential than carbon dioxide (CO_2) on the global warming potential (GWP) scale.[3] This gas and other lower hydrocarbons (C_2H_6, C_3H_6, *etc.*) are potential raw materials for the chemical industry. In fact, these compounds could be permanently converted into their corresponding chemical liquid products through efficient processes. From an economic perspective, the oxidation approaches for the functionalization of lower alkanes ($n \leq 3$) offer an attractive alternative compared to conventional gas-to-liquid processes because they do not rely on the intensive energy formation of syngas.[4] However, due to low reactivity, the selective conversion of alkane to alcohol is particularly difficult. A potential solution for this challenge resides in the design and materialization of a discrete molecular catalyst that activates and functionalizes C–H bonds of the corresponding alkane. Since the emergence of Shilov's approaches based on the activation and catalytic reactions of saturated hydrocarbons in the presence of transition metal (TM) complexes, the reactivity of alkanes has received much attention, and at the same time, the coordination of ligands to these TMs has also facilitated various spectacular catalytic transformations (Suzuki, Miyaura, and Heck cross-coupling reactions).[5,6] In modern organometallic chemistry, the knowledge of ligand tuning remains one of the most powerful concepts for regulating the catalytic properties of TM centers and predicting catalytic activity. Since the synthesis and the isolation of the first free N-heterocyclic carbene (NHC) by

[a]*Computational and Theoretical Chemistry Unit, Department of Chemistry, Faculty of Science, University of Douala, P.O. Box 24157, Douala, Cameroon. E-mail: jean.monfils@yahoo.fr*

[b]*Physical and Theoretical Chemistry Laboratory, University of Yaoundé I, P.O. Box 812, Yaoundé, Cameroon. E-mail: adjieufack21@gmail.com*

† Electronic supplementary information (ESI) available. See DOI: https://doi.org/10.1039/d4ra03893b

Arduengo, these compounds have become universal ligands in coordination chemistry.[7] They easily bind to all TMs with a low or high oxidation degree. Due to their specific coordination chemistry, NHC stabilizes and activates metal centers in key areas (medicinal,[8] luminescent,[8] functional material applications[8] and catalysis[9–11]…). Despite this great interest in NHCs, detailed knowledge of the molecular mechanism and factors underlying their catalytic activity of hydrocarbon oxidation is still limited. In addition, the improvement of catalysts, therefore, remains in the test procedure, which can be done with multiple errors after the modification of the structure, and the resulting catalyst induces multiple steps until the reaction takes place. Such a fact is not adequate for a concept that is increasingly required by the scientific community: green chemistry. However, these trends have favored the development of diimidazolium salts as a precursor of the chelating bis-N-heterocyclic carbene (bis(NHC)) ligand. The corresponding complexation strategies allow the synthesis of a wide range of chelating bis(NHC) ligand metal complexes with variable structural and electronic properties. These properties offer the unique reactivity not found in their monodentate homologues for the activation and functionalization of the C–H bond (oxidation) of alkanes. Among these bidentate bis(NHC) ligands, the CH_2-bridged bis-N-heterocyclic carbene ligands of bis(imidazole-2-ylidene) unit is the most common.

The pioneering work on the generation of chelating dicarbene stabilized metal complexes with well-defined structures was carried out by Herrmann and co-workers.[12,13] Subsequently, a wide range of chelating metal dicarbene complexes has been prepared from diimidazolium salts. Palladium is a metal exploited in a plethora of C–C coupling reactions (Mizoroki–Heck reaction, Suzuki–Miyaura reaction, Sonogashira coupling reaction), and many works related to palladium are summarized in these reviews.[13–16] In addition, more than two decades ago, the Strassner group contributed to the conversion of methane and propane into liquid products by catalytic activation with an efficient functionalization of their C–H bond in the presence of palladium(II) complexes [Pd(II)bis(NHC)] and trifluoroacetic acid (HOTFA).[17] These complexes lead to higher reactivity and catalyst stability compared to palladium(II) catalysts without NHC ligands.[18]

Furthermore, a sub-class of bis(NHC) ligands, so-called abnormal dicarbenes, which bind the metal through the imidazole C_4 or C_5 (C_{aNHC}) site (Scheme 1(a)), has been investigated recently by Khlebnikov and co-workers.[19] Their experimental studies have suggested that the heavy metal center was a stronger Lewis base when coordinated by the C_{aNHC} site of C_4-bound bis-N-heterocyclic carbene (bis(aNHC)) ligand[20] compared to C_{nNHC} (Scheme 1(b)) ones. However, the contribution of iodide ions has not been clearly elucidated, as well as their involvement in the reactivity of the complexes in the same works. Independent of the exact bond description between C_{aNHC} of bis(aNHC) ligand with TM, the substantially higher donor strength of the C_{aNHC}–metal bond is expected to have a strong impact on the catalytic activity of the coordinated metal center. This fact may disclose new applications in the catalysis field. It is, therefore, of utmost importance to combine the specific metal with the appropriate halide ions. Thus, Strassner's work on the influence of the counter-ion in the catalytic methane C–H bond activation mechanism by successively combining the halides Cl^-, Br^-, and I^- with the Pd normal complex showed that for iodide, no activation could be observed.[21] This point of view initiated by Strassner, and thus the authorship of the normal chelating complex is conceded to him, has given rise to a lot of hype concerning the emanation of the reactivity of the complex, which would be closely related to the combination of the metal, type of ligand and halide adopted.[12–22] However, in the case of platinum metal, for example, normal and abnormal complexes, overall, acquired in practical applications have the effect of spurring a remarkable amount of experimental and theoretical works focused on the understanding Pt–C_{NHC} and Pt–X bonds.[19] A cumulative extension to this study has also highlighted other transition metals.[19–22] The initial hypothesis based on the simple σ-donor character of bis(NHC) is now abandoned. To understand the electronic details and bonding properties of the M–C_{HNC} bond and their role in catalysis, both d → π*M to NHC π*-

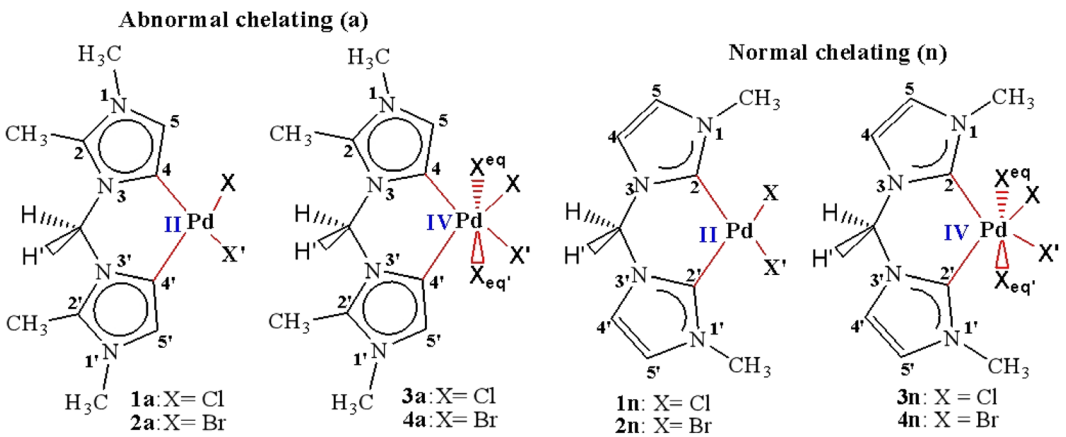

Scheme 1 Palladium(II and IV) CH_2-bridged bis-N-heterocyclic carbene complexes featuring abnormal (**1a**, **2a**, **3a**, and **4a**) and normal bonding (**1n**, **2n**, **3n**, and **4n**).

back donation as well as $\pi \rightarrow d_{NHC}$ to M π-donation must be considered. To date, actual comprehension of the structural architecture of these complexes necessary to explain the catalytic properties of reactions remains an incongruous topic. Our recent investigations indicate that the stability and reactivity of the metal–bis(NHC) complexes are not only related to their electronic properties but also to the coordination mode adopted[23] and the oxidation state involved, $M^0/M^{II}/M^{IV}$.[24] Whereas for their monodentate counterparts benefiting from Tolman's studies,[9] topological properties have been clarified. The idea of increasing the oxidation number of palladium from +2 to +4 in different complexes can be an informative index to inspect the favoured complexation process contributing to the bond activation mechanism. Exhibiting the exponential reactivity and given their ability to operate as catalysts for alkane C–H activation, we chose Strassner's complexes as a starting point for our explorations.

The aim of this study is to investigate the impact of the ligand's coordination mode and the palladium's oxidation state on the chemical bond between the bis(NHC) ligand and palladium. Additionally, the study aims to establish design criteria for new catalysts of bis(NHC)$Pd^{IV}X_4$ complexes based on electronic parameters using density functional theory analysis. This study is motivated by the fact that many similar normal-type complexes (Strassner's chelating type complex) have been reported to date, but the nature of the $C_{carbene}$–Pd and Pd–halogen bonds, the oxidation state of palladium and their role in catalytic reactivity have not been clearly understood. In addition, the study of these properties in the case of abnormal-type complexes is unprecedented.

2 Computational details and background theory

2.1 Computational details

The geometry of different complexes was optimized using Gaussian 16 program[25] at the Density Functional Theory (DFT) using the B3PW91 functional,[23,26] LANL2DZ basis set for Pd, Cl, and Br, and the 6-31G(d) basis set for H, C, and N atoms. Frequency calculations were carried out at $T = 298.15$ K and $P = 1$ atm, in which all vibrational frequencies exhibited a real mode, confirming that these complexes are minima on the potential energy surface. To explain the rationality of the B3PW91 functional, additional calculations were carried out by employing the ωB97X-D with def2-TZVP basis set. Each thermodynamic state function (enthalpy, entropy, Gibbs free energy, and binding energy) was evaluated at $T = 298.15$ K and $P = 1$ atm (standard conditions). The QTAIM analysis and ELF electron population were carried out with the aid of Multiwfn 3.3.8 program[26] to examine the nature of bonds in terms of electronic structure and bonding properties. To quantify the binding interactions around the metal centre, NBO, as implemented in the Gaussian 16 program,[25] was developed at the B3PW91/6-31G(d)/Lanl2DZ level on optimised complexes. Finally, to obtain the density of states (DOS), partial density of states (PDOS) and overlap population density of states (OPDOS) spectra based on MOs, Multiwfn 3.3.8 program[26] was used.

2.2 Background theory

Conceptual DFT (CDFT) measures the reactivity and stability of molecular systems by extracting chemically relevant concepts from the DFT in terms of global reactivity descriptors (GRDs).[27] The global electrophilicity ω, was estimated by applying the following formulas linked to the electronic chemical potentials (μ) and chemical hardness (η) of the studied complexes; $\mu_{cp} = -\frac{IP + EA}{2}$ and $\eta = \frac{IP - EA}{2}$. The values of μ and η were then used for the calculation of ω *via* the formula $\omega = \frac{\mu_{cp}^{\ 2}}{2\eta}$.[27] Electronic parameters, IP ($-\varepsilon_{HOMO}$) and EA ($-\varepsilon_{LUMO}$), defined as the first vertical ionization potential and electronic affinity, respectively, and E_{gap} (ε_{LUMO}–ε_{HOMO}) are used to discuss the chemical stability through electron transfer within the complexes according to Koopmans' theorem.[28,29] In quantum chemical topology, the properties of one-density scalar functions are used to discuss the strength and nature of chemical bonding in molecules.[30,31] This approach provides a partition of the function into non-overlapping atomic regions, so-called basins. The gradient field is characterized by its critical points (CPs) (where $\rho(r) = 0$) and their connectivity. CP can be either local maxima, minima or saddle points. In the QTAIM approach, the topological atom is defined as the union of a nucleus and its basin. Among the saddle points, a bond critical point (BCP) has a crucial role because the values of some descriptors at the BCP are related to the nature of the chemical bond. The electron density $\rho(r)$ at the BCP is typically larger than 0.20 e $bohr^{-3}$ in shared-shell interactions, in other words, covalent bonds, and smaller than 0.10 e $bohr^{-3}$ in closed-shell (ionic) interactions. When the Laplacian of the density ($\nabla^2\rho(r)$) at the BCP is negative, the local concentration of charge indicates a shared-shell interaction. In contrast, if $\nabla^2\rho(r)$ is positive, there is a depletion of charge typically characterizing a closed-shell interaction. Due to the complexity of the nature of bonding interactions, another descriptor often used in QTAIM to distinguish shared-shell, closed-shell and intermediate bonding regimes is the ratio ($|V(r)|/(G(r))$), based on the potential energy density ($V(r)$) and the kinetic energy density ($G(r)$) at the BCP. When this ratio is smaller than 1, the kinetic energy density is the leading term, and electrons are destabilized close to the BCP; thus, no covalency is expected (pure ionic bond). The intermediate bond regime can be observed when the ratio is greater than 1 and less than 2 ($1 < |V(r)|/(G(r) < 2$). The energy density $H(r)$ summarizes the mechanics of a bonding interaction. $H(r)$ is negative for interactions with significant electron sharing, with its magnitude reflecting the covalence of the interaction.[32] In line with this topological analysis, the bonding interaction between atoms was examined using the natural bond orbital (NBO) analysis.[33] The second-order perturbation energy stabilization (E^2) for each donor NBO(i) and acceptor NBO(j) estimated data is defined as follows:[33]

$$E^{(2)} = \Delta E_{ij} = q_{ij}\frac{F^2(i,j)}{\varepsilon_j - \varepsilon_i}$$

where, q_{ij} represents the donor orbital occupancy, ε_j and ε_i are diagonal elements, and $F^2(i, j)$ is the off-diagonal NBO Fock matrix elements.

3 Results and discussion

3.1. Geometrical analysis

In order to predict the chemical reactivity of chelating bis(NHC) complexes towards the C–H bond activation of organic compounds, it is necessary to perform calculations at an appropriate theoretical level. Scheme 1 shows the eight bis(NHC) complexes, while Table 1 summarizes some key structural parameters (bond distances, valence, and dihedral angles) evaluated at the B3PW91//LANL2DZ/6-31G(d) level. Two chelating modes, normal (**1n**, **2n**, **3n**, and **4n**) and abnormal (**1a**, **2a**, **3a**, and **4a**), which correspond to different oxidation states (+2 and +4) of palladium are chosen for this investigation.

From Table 1, the distance of C_{nNHC}–Pd (2.064 Å) and C_{aNHC}–Pd (2.019 Å) bonds are 0.071 and 0.022 Å greater in tetrachloride complexes (**3n** and **3a**) compared to the dichloride (**1n** and **1a**) ones. A similar trend is observed in the case of bromide complexes in which the $C_{carbene}$–Pd distance [C_{nNHC}–Pd; 2.092 Å (**4n**) and C_{aNHC}–Pd; 2.039 Å (**4a**)] experienced a bond lengthening of 0.089 and 0.003 Å as compared to **2n** and **2a**, respectively. In addition, the distance of C_{nNHC}–Pd and C_{aNHC}–Pd bonds are longer in bromide than chloride complexes, with a slight increase occurring when passing from normal to abnormal complexes. All these observations suggest that the palladium (II and IV) center is a stronger Lewis or Brønsted base when coordinated by bis(aNHC) abnormal ligands as opposed to bis(nNHC) normal. This may be attributed to a more pronounced zwitterionic bonding of bin(aNHC), comprising an anionic vinyl-type fragment (C=C) for palladium coordination and a cationic NCN amidinium residue for intramolecular charge compensation.[19] Irrespective of the exact $C_{carbene}$–Pd bond description, the substantially higher donor power of bis(aNHC) is expected to have a strong impact on the catalytic activity of the coordinated palladium center.

With regard to the Pd–X bonds for dihalide complexes, the Pd–Br bond (2.549 Å in **2n** and 2.593 Å in **2a**) is notably longer than the Pd–Cl bond in the **1n** and **1a** complexes by approximately 0.137 and 0.141 Å, respectively (see, Table 1). Collectively, this Pd–X bond length analysis may hence point to a virtually different *trans* influence of the two chelating bis(NHC) ligands, although steric factors need to be considered as well, and a slightly greater *trans* influence coupled to the large size nuclei of bromide compared to chloride. This means that the repulsion of the halide from the palladium(II) coordination sphere due to the presence of a CH_3 substituent at peripheral nitrogens (Scheme 1) is expected to be more pronounced in the bis(nNHC) than in the bis(aNHC) ligand. The same trends are observed for tetrahalide complexes for which the Pd–X^{eq} equatorial bond in **3n** and **3a** (Pd–Cl^{eq} close to 2.44 Å) and **4n** and **4a** (Pd–Br^{eq} close to 2.60 Å) remains nearly

Table 1 B3PW91//LANL2DZ/6-31G(d) and B3PW91/def2TZVP (in bold) geometry parameters of normal (**1n**, **2n**, **3n**, and **4n**) and abnormal (**1a**, **2a**, **3a**, and **4a**) complexes

	Palladium(II)				Palladium(IV)			
Chelating-type	Normal		Abnormal		Normal		Abnormal	
Complexes	**1n**	**2n**	**1a**	**2a**	**3n**	**4n**	**3a**	**4a**
C_j–Pd	1.993	2.003	1.997	2.009	2.064	2.092	2.019	2.039
	1.993	**1.996**	**1.981**	**1.990**	**2.034**	**2.055**	**1.994**	**2.010**
$C_{j'}$–Pd	1.993	2.003	1.997	2.009	2.064	2.092	2.019	2.039
	1.993	**1.996**	**1.981**	**1.990**	**2.034**	**2.055**	**1.994**	**2.010**
Pd–X′	2.412	2.549	2.452	2.593	2.436	2.595	2.451	2.603
Pd–$X^{eq'}$	**2.342**	**2.478**	**2.363**	**2.499**	**2.350**	**2.498**	**2.371**	**2.519**
	—	—	—	—	2.443	2.611	2.460	2.621
	—	—	—	—	**2.333**	**2.494**	**2.325**	**2.484**
Pd–X′	2.412	2.549	2.452	2.593	2.436	2.595	2.451	2.603
Pd–$X^{eq'}$	**2.342**	**2.478**	**2.363**	**2.499**	**2.350**	**2.498**	**2.371**	**2.519**
	—	—	—	—	2.439	2.611	2.431	2.596
	—	—	—	—	**2.336**	2.501	2.354	2.508
C_j–Pd–$C_{j'}$	86.1	85.7	88.9	88.3	86.5	86.3	89.6	89.1
	85.6	**85.2**	**88.5**	**87.9**	**86.1**	**86.8**	**89.2**	**89.1**
X–Pd–X′	93.2	92.8	96.5	95.4	88.8	87.0	89.6	92.9
X^{eq}–Pd–$X^{eq'}$	**92.8**	**93.9**	**95.4**	**95.2**	**88.9**	**88.0**	**94.1**	**92.5**
	—	—	—	—	177.5	180.0	172.6	174.7
	—	—	—	—	**177.4**	**177.9**	**173.3**	**173.4**
X–X′–$C_{j'}$–C_j	0.0	0.0	0.0	0.0	0.0	0.0	0.0	0.0
X^{eq}–$X^{eq'}$–$C_{j'}$–C_j	0.0	0.0	0.0	0.0	0.0	0.0	0.0	0.0
	—	—	—	—	53.4	54.2	48.8	49.4
	—	—	—	—	53.3	54.2	49.6	49.4
H^{endo}–C–H^{exo}–Pd	180.0	180.0	180.0	180.0	180.0	180.0	180.0	180.0
				180.0	**180.0**	**180.0**	**180.0**	**180.0**

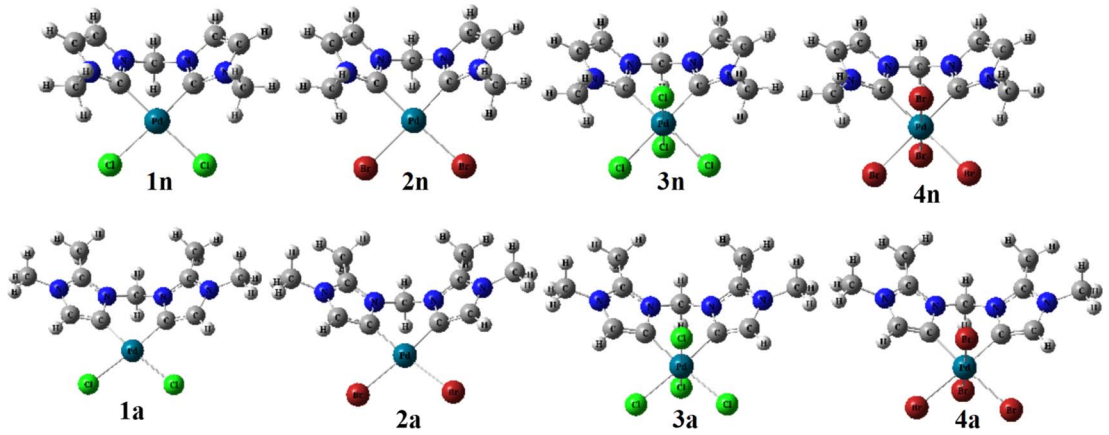

Fig. 1 B3PW91//LANL2DZ/6-31G(d) optimized geometries of abnormal (**1a**, **2a**, **3a**, and **4a**) and normal (**1n**, **2n**, **3n**, and **4n**) complexes.

unchanged when switching from the normal to the abnormal model. However, these equatorial bonds are longer compared to the axial ones (Pd–X) within Pd^{IV} complexes (Table 1).

In order to guarantee the accuracy and validity of our geometric results and the level of theory adopted, we have initially compared the Pd–X and $C_{carbene}$–Pd bond distances within the complexes from the available experimental data for the analogues. In agreement with the experimental data, the computations reproduced the strong chelating bond between the ligand and metal. Most of our calculated geometric data of the C_{nNHC}–Pd, Pd–Cl bonds agree very well with the experimental data for the **1n** complex.[21] The maximum differences between X-ray data and our results for **3n** complex in C_{nNHC}–Pd, Pd–Cl, and Pd–Cl^{eq} bond lengths are just 0.045, 0.055, and 0.127 Å,[24] respectively. This discrepancy could justify either the difference between the solid (X-ray data) and gas (our work) phases or the level of calculation. However, the lack of data from other complexes means that this comparison is limited to **1n** and **3n**. Otherwise, to more accurately reflect our findings in relation to the discrepancy observed in previous comparisons of C_{nNHC}–Pd, Pd–Cl, and Pd–Cl^{eq} bond distances with experimental values on the **3n** complex, we have implemented a revised calculation methodology. This employs the B3PW91/def2TZVP approach in the same gas phase. So, it is particularly instructive to compare the geometric data at the B3PW91/LanL2DZ/6-31G(d) level of theory with B3PW91/def2TZVP for all the complexes. Table 1 shows that the $C_{carbene}$–Pd bond distance is identical within standard deviations in both approaches, averaging to 1.99 (**1n**) and 2.00 Å(**2n**) in normal and 1.99 (**1a**) and 2.00 Å(**2a**) in abnormal dihalide complexes. Similarly, the Pd–X bond distances are statistically equal, averaging 2.38 (Pd–Cl:**1n**) and 2.51 Å (Pd–Br:**2n**) in normal and 2.41 (Pd–Cl:**1a**) and 2.55 Å (Pd–Br:**2a**) in abnormal. Similar results were found for tetrahalide complexes but with much longer bond distances (see Table 1). This analysis of bond lengths indicates that the two levels of theory exhibit virtually identical geometric data, thereby highlighting a relative choice of level of theory to adopt. Beyond all considerations, we finally adopted the 6-31G (d) basis, which is more sophisticated and better suited to optimising the geometry of transition metal complexes, to the detriment of the def2TZVP basis, although the latter is more efficient in terms of calculation time.

Focusing on the angles, the pallado-chelation of the bis(aNHC) and bis(nNHC) ligands coupled to both halides (Cl^- or Br^-) forms a six-membered metallacycle in all complexes. Table 1 shows the angles of the computed complexes. From Table 1, we can see that the C_j–Pd–$C_{j'}$ bite angle and X–Pd–X′ of the chelating dicarbene around the Pd center are slightly smaller than 90°. This makes them well-suited for stabilising square-planar and octahedral coordination geometries for Pd(II) and Pd(IV), respectively. The X–X′–$C_{j'}$–C_j (0.0°) and H′–C–H–Pd (180.0°) dihedral angles form two perpendicular planes as an indicator for a bisector symmetry containing a C_{2v} pseudo-symmetry axe, which keeps the Pd, $C_{bridged}$, H′, and H atoms invariant in Pd^{II} complexes or the X^{eq}, $X^{eq'}$, Pd, and $C_{bridged}$ atoms in the Pd^{IV} ones (Fig. 1).

3.2. Reactivity and thermodynamic stability evaluation

The analysis of the reactivity indices defined within the framework of the conceptual DFT (CDFT) is an important tool for evaluating the reactivity of chemical species. Table 2 presents the electronic chemical potential (μ), chemical hardness (η), and global electrophilicity (ω). As can be seen from Table 2, the ω values of the dihalide complexes (**1n**, **2n**, **1a**, and **2a**) are smaller than those of the tetrahalide complexes (**3n**, **4n**, **3a**, and **4a**), which range from 10.11 to 15.51 eV. From this, it can be inferred that the $LaPd^{IV}X_4$ or $LnPd^{IV}X_4$ tetrahalide palladium complexes exhibit preferential electrophilic behavior for the C–H bond activation processes in the following order: **3a** > **3n** > **4a** > **4n**. This justifies the good electrophilic character of the tetrachloride complex for the catalytic C–H bond activation, as experimentally explored by McCall.[24] All these complexes are strong electrophiles according to the electrophilicity scale, which divides chemical compounds into strong (ω > 1.5 eV) and moderate (ω > 0.8 eV) electrophiles.[34] Based on this electrophilic criterion, **3a** would have the highest catalytic activity.

Regarding the thermodynamic stability, the values of ΔE_{bind} are negative in all cases, and therefore, indicate that bis(NHC) ligand stabilizes the $C_{carbene}$–Pd bond. In addition, this value of

Table 2 Electronic chemical potential (μ), chemical hardness (η), global electrophilicity (w), enthalpy (ΔH^0), Gibbs free enthalpy (ΔG^0), entropy (ΔS^0) and complexation energy of normal (**1n**, **2n**, **3n**, and **4n**) and abnormal (**1a**, **2a**, **3a**, and **4a**) complexes at the B3PW91//LANL2DZ/6-31G(d) level of theory

Complex	μ (eV)	η (eV)	ω (eV)	ΔG^0 (kcal mol^{-1})	ΔH^0 (kcal mol^{-1})	ΔS^0 (kcal mol^{-1})	E_{bind} (kcal mol^{-1})
1n	−3.40	2.24	2.59	−45.20	−59.0	−0.046	−58.4
2n	−3.30	1.95	5.59	−38.8	−25.0	−0.05	−20.8
1a	−2.94	1.74	2.48	−44.6	−57.7	−0.044	−57.1
2a	−2.86	1.60	2.56	−33.9	−46.4	−0.042	−45.8
3n	−3.69	0.51	13.37	−102.3	−118.6	−0.055	−118.0
4n	−3.96	0.78	10.11	−80.6	−96.9	−0.067	−96.3
3a	−3.77	0.46	15.51	−111.7	−126.8	−0.050	−126.1
4a	−4.04	0.72	11.29	−92.2	−107.9	−0.052	−107.3

ΔE_{bind} increases from abnormal to normal chelating mode complexes due to the less π-backbonding ability of the metal. It is also important to note that the halide ions affect the strength of the $C_{carbene}$–Pd bond. Concerning the Gibbs free energies, their negative values reveal that all these complexes exist and are stable (Table 2). Furthermore, the highest value of Gibbs free energy (−33.9 kcal mol^{-1}) is recorded for **2a**, while the smallest one (−111.7 kcal mol^{-1}) is noted for **3a** (more stable than the others, see Table 2).

3.3. Frontier orbitals and density of state analysis

To better achieve the catalytic activity of all complexes through their intrinsic electronic bond properties, it is important to study the effective influence of C_{nNHC}–Pd, C_{aNHC}–Pd, and Pd–X bonds since the reactivity and stability discussed above (see Section 3.2) are affected by the presence of molecular bond orbital interactions. For that, we resorted to boundary orbital analysis in which each complex is divided into Pd^{i+} cation, halide ion (X^-), and carbenic carbon (C_{nNHC} or C_{aNHC}), respectively. The atom contributions and the frontier molecular overlap compositions in each complex are given in Fig. 2 and 3. The analysis of HOMO clearly presents an electron density distribution preferentially located on the Pd^{II} center with a moderate HOMO energy close to −5.40 and −4.50 eV (Fig. 2) for the Pd^{II} normal and abnormal (except **2a**, −4.46 eV) chelating models, respectively. Whereas, in the case of Pd^{IV} complexes, this electron density distribution entirely affects the first coordination sphere with almost the same HOMO energy as Pd^{II}. Following these previous observations, LUMO presents a high contribution deallocated preferentially on both imidazole rings with an energy close to −1.20 and −3.250 eV in Pd^{II} and Pd^{IV} complexes, respectively (Fig. 2 and 3). In addition, the $E_{LUMO-HOMO}$ gap of **2n** (3.90 eV) and **2a** (3.20 eV) Pd^{II} bromide complexes is low compared to that of Pd^{II} chloride counterparts (**1n**, 4.47 eV and **1a**, 3.47 eV). In line with this analysis, the reversible fact was obtained upon the Pd^{IV} complexes for which the lower $E_{LUMO-HOMO}$ values were observed for **3n** (1.01 eV) and **3a** (0.91 eV) chloride complexes compared to bromide ones (Fig. 3). These observations highlight the lower kinetic stability of bromide Pd^{II} and chloride Pd^{IV} complexes, which correspond to greater preferential reactivity of each complex group. The preferential reactivity observed for bromide Pd^{II} and chloride Pd^{IV} complexes could explain the choice of their use as catalysts for the direct C–H bond activation and functionalization reactions of alkane,[10,11,21] aromatic, alkene and benzylic aliphatic.

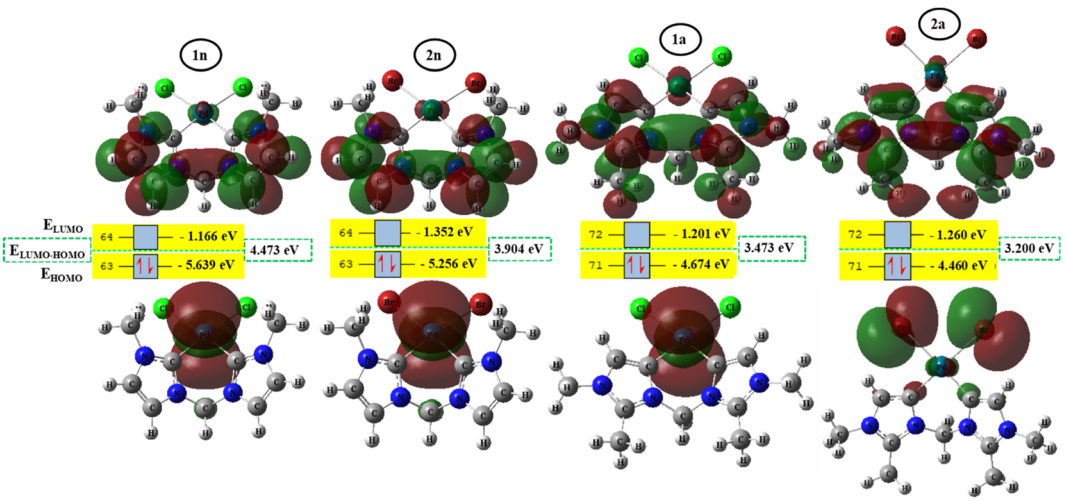

Fig. 2 HOMO and LUMO isosurfaces (isovalue:0.02) of normal (**1n**, **2n**, **3n**, and **4n**) complexes at B3PW91//LANL2DZ/6-31G(d) level of theory.

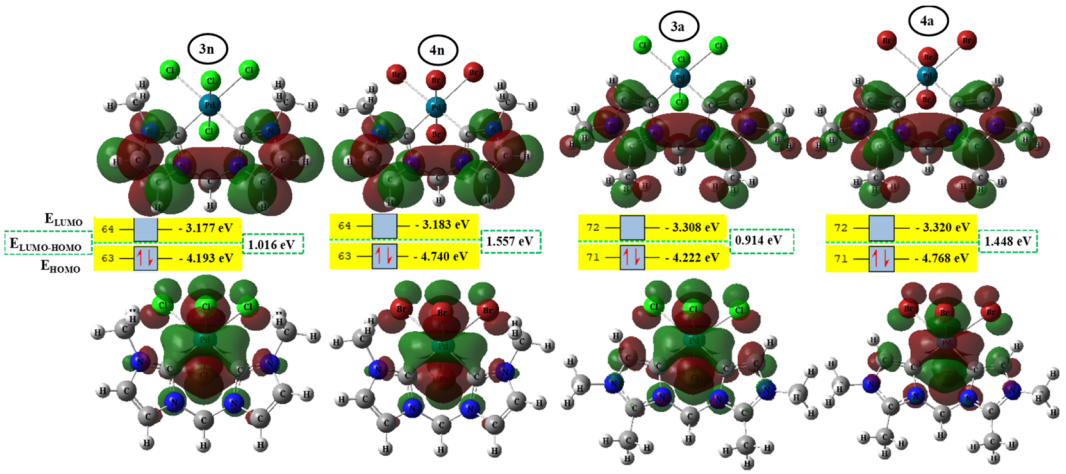

Fig. 3 HOMO and LUMO isosurfaces (isovalue: 0.02) of abnormal (**1a**, **2a**, **3a**, and **4a**) complexes at B3PW91//LANL2DZ/6-31G(d) level of theory.

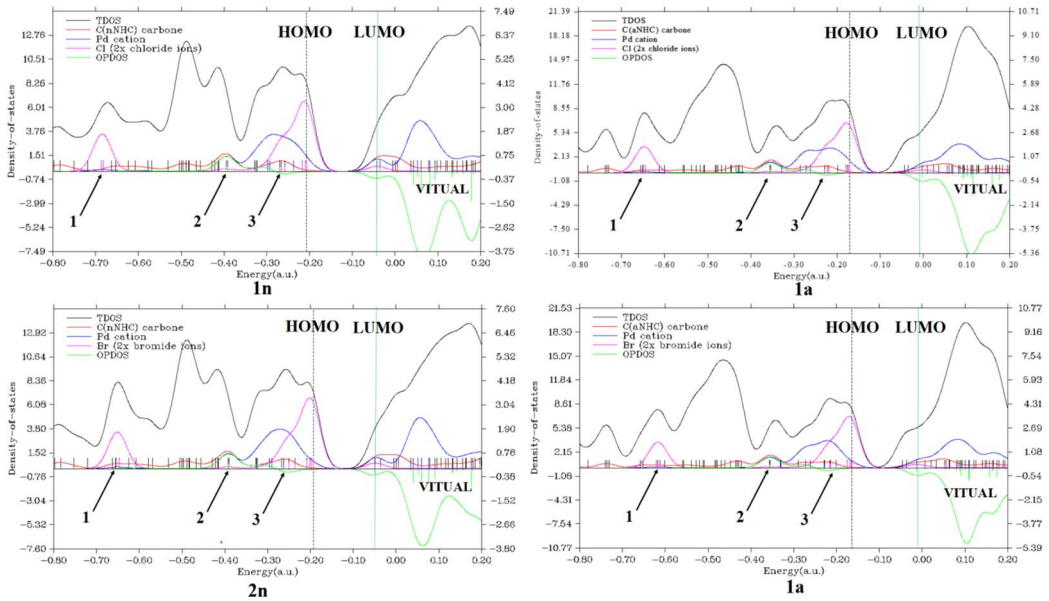

Fig. 4 . Total (black), partial [red (C_{jNHC}), blue (Pd^{2+}), and magenta [(ClvBr)], and overlap [green, between C_{jNHC} and Pd^{2+} or $Pd^{2+}$and X(X = ClvBr) basis functions] density-of-states map of bis(aNHC)[bis(nNHC)]$Pd^{II}PdX_2$ complexes.

Secondly, considering the DOS map displayed in Fig. 4 and 1S,† it is important to know that each discrete vertical line corresponds to a molecular orbital (MO) energy level.[35] In our case, the red, blue, and magenta curves represent the PDOS of C_{nNHC} or C_{aNHC} carbon, Pd^{II} or Pd^{IV} cation and Cl or Br ion, respectively. As can be seen from Fig. 4, the TDOS, PDOS and OPDOS information analysis of the energy levels allows us to observe three similar positions in each complex. The magenta PDOS curve, which is linked to the energetic density of states of halides (Cl^- in **1n**, **1a** and Br^- in **2n**, **2a** complexes), closely follows the black line (TDOS) in the regions ranging from −0.75 to −0.65 a.u (arrow 1 point) and from −0.35 to −0.15 a.u (arrow 3 points). These regions correspond to σ^* (3 s) and π^*(3p) orbitals, respectively, in all complexes. The fact that OPDOS (green curve) in these regions (arrow 1 and 3 points) is almost zero indicates a nonbonding interaction character[35] between the Pd^{2+} cation and any halide in the corresponding complex. Furthermore, according to OPDOS diagrams, in their positive region close to −0.40 a.u (arrow 2 points) for **1n**, **2n**, **1a** and **2a** dihalide complexes, a π-bonding interaction character is established between C_{nNHC} and Pd^{2+} for normal complexes and C_{aNHC} and Pd^{2+} for abnormal ones.

Concerning the Pd^{IV} tetrahalide complexes, Fig. 1S† clearly shows the orbital characteristics in different energy ranges. Two main compositions of the MOs around −0.37 a.u (arrow 1 point) and −0.18 a.u (arrow 2 point) would be the bonding orbitals of the Cl^-vBr^-(magenta curve) with the Pd^{4+} atoms (blue curve) and the π-orbitals of C_{nNHC} or C_{aNHC} with Pd^{4+} elements, respectively. Inspection of the green OPDOS curve in these sites, which expresses the bonding character between Cl^- (in **3n** and

3a) or Br^- (in **4n** and **4a**) halides with Pd^{4+} cation, and C_{nNHC} or C_{aNHC} atoms with Pd^{4+}, on the other hand, suggest that their orbitals are very important for the stabilisation of $C_{aNHC}\cdots Pd$, $C_{aNHC}\cdots Pd$ and $Pd\cdots X$ interactions. This observation is related to the fact that OPDOS has a positive value in these ranges (Fig. 1S†). For all virtual MOs, the OPDOS curve lies in the negative region and shows an anti-bonding character in this region. This is due to the unfavourable overlap in the orbital phase, as can be seen on the LUMO isosurface (Fig. 4 and 1S†).

3.4. Electronic and bonding properties

3.4.1. NBO analysis. The analysis of electronic interactions allows us to predict the bonding properties within each complex. In fact, the natural atomic orbital (NBO) analysis provides access to the natural charges of atoms, natural atomic orbitals, and donor–acceptor interactions at the second-order perturbation within different complexes. We have performed NBO calculations on different complexes as well as the ones of isolated fragments [bis(nNHC) or bis(aNHC) and $Pd^{II}X_2$ or $Pd^{IV}X_4$ (halogens-metallic) moieties]. NBO charges of C_{jNHC}, Pd^{II}, and Pd^{IV} in each complex and isolated fragment are listed in Table 1S.† Table 1S† shows that for the bis(aNHC) [bis(nNHC)]$\cdots Pd^{II}X_2$ interaction, the charge difference between the ligand and halogens metallic fraction is large in the abnormal chelating model (0.71 and 0.62 Q/e for **1a** and **2a**, respectively) compared to normal ones (0.39 and 0.30 Q/e for **1n** and **2n**, respectively) in Pd^{II} complexes. Table 1S† also shows that the coordination between bis(aNHC) or bis(nNHC) and $Pd^{II}X_2$ or $Pd^{IV}X_4$ halogens-metallic moiety induces a relative increase in charge of the C_{aNHC} (C_{nNHC}) atom. Its value attains +0.18 Q/e in **1n**(**2n**), and +0.19 Q/e in **1a**(**2a**), respectively. A notable decrease in Pd^{2+}charge ranging from −0.62 to −0.49 Q/e is observed and progresses when passing from abnormal to normal chelating mode in the following order **1a** < **1n** < **2a** < **2n**. The same observations are recorded in **3n** and **4n** tetrahalide complexes with the charge of C_{nNHC}, which increases by about +0.25 Q/e while the one of Pd^{4+} decreases by −0.52 Q/e (Table 1S†). Thus, it is now well known that the mode of chelation and the halide ion are influenced reciprocally by the oxidation state of the palladium atom. However, the interaction charge transfer is less than 1 Q/e (charge unit) in all cases, suggesting no covalent interaction. Fig. 2S† shows the existence of the electric dipole between carbene moiety and metallic fragment, which is generated by the dissymmetry of the shared charge distributions between C_{aNHC}(C_{nNHC}) and Pd atoms. Such facts highlight an ionocovalent character of this interaction that we can model as: bis(NHC)$^{-2\delta}\cdots PdX_i^{+i\delta}$. An investigation of the natural electronic configuration in localized Lewis-like terms of the palladium cations in different complexes is admitted by explaining the electronic cation environment. Table 2S† summarizes the natural population orbital (NPO) of palladium cation in different complexes and isolated state as an effective valence natural electron configuration. Although the occupancies of the NPO are non-integer in the molecular environment, starting from $4d^8$, the effective atomic configurations show an electron depletion ranging from 0.68 to 1.07 e. This electron depletion reveals the acceptor character of the palladium ion, which is more pronounced in dihalide than tetrahalide complexes and presumably adopts a $4d^9$ transition metal pattern. To examine the hybridization type of bonds around the palladium cation coordination, the percentage of polarizability and their natural hybrid atomic orbital (NHAO) contributions are given in Tables 3 and 3S.† NBO shows that they are mainly composed of s-type, p-type, and d-type orbitals corresponding to $C_{jNHC}\cdots Pd$ and $Pd\cdots X$ σ-bonding orbitals. Table 3 clearly reveals that the $C_{NHC}\cdots Pd$ σ-bonding is greatly polarised towards the C_{NHC} atom, with the contribution ranging from 23.13–32.08% for the Pd cation and 69.55–76.87% for the C_{NHC} atom. This last contribution is more pronounced in Pd^{II} than Pd^{IV} complexes independently of chelating mode and increases as follows, $C_{aNHC} < C_{nNHC}$. Concerning the $Pd\cdots X$ bonding, similar observations summarized in Table 3S† indicate that σ-bonding orbitals are more polarised towards the halide ion (17.26–32.99% and 67.01–81.66% contribution from Pd^{2+}(Pd^{4+}) and Cl^- (Br^-), respectively). Collectively, the NHAO composition (see Table 3 and 3S†) highlights that the palladium atom (in $Pd\cdots X$ and $C_{NHC}\cdots Pd$ bonding interaction) is sdp^2 hybridized (*e.g.* s(25.23%), p(46.79%), d(27.98%) for **1n**, see Table 2S†) corresponding to the qualitative concept of interacting sdp^2 hybrids. The "d" character of palladium cation in these hybridizations increases when going from Pd^{II} to Pd^{IV} complexes and decreases when passing from abnormal to normal complexes. After all these NHAO observations, we point out that bromine preferentially mediates the oxidation of Pd^{II} to Pd^{IV}. This fact could be beneficial for their use in catalysing the alkane C–H

Table 3 Natural hybrid orbital (NHO) analysis of the C_{jNHC}–Pd bond

Comp.		Occu.	Polarizability		Hybridization	
			Pd	C_{jNHC}	Pd	C_{jNHC}
1	**n**	1.82	23.13%	76.87%	s(25.23%), p(46.79%), d(27.98%)	s(40.98%), p(59.02%)
	a	1.81	23.46%	76.54%	s(25.26%), p(45.91%), d(28.83%)	s(37.80%), p(62.20%)
2	**n**	1.82	23.18%	76.82%	s(25.58%), p(46.00%), d(28.42%)	s(41.24%),p(58.76%)
	a	1.81	23.52%	76.48%	(25.59%), p(45.17%), d(29.24%)	s(37.97%), p(62.03%)
3	**n**	1.80	31.08%	68.92%	s(18.64%), p(46.79%), d(34.57%)	s(37.26%), p(62.73%)
	a	1.78	32.38%	67.62%	s(18.41%), p(45.20%), d(36.38%)	s(34.04%), p(65.95%)
4	**n**	1.82	30.45%	69.55%	s(18.73%), p(46.11%), d(35.16%)	s(38.16%), p(61.83%)
	a	1.80	32.08%	67.92%	s(18.22%), p(44.53%), d(37.24%)	s(34.69%), p(65.31%)

bond activation reaction. Munz and co-workers illustrate consistent reaction mechanisms to this end.[11] In addition to deciphering possible donor–acceptor NBO interactions exclusively between bis(jNHC) ligands and PdXi metallic moiety, the stabilization energies (E^2)[33] were calculated based on the second-order perturbation theory, and the obtained results are plotted in Fig. 3S.† From Fig. 3S,† LP(4)Pd → π*(C_{aNHC}–C_5) (abnormal) and LP(4)Pd → π*(C_{nNHC}–N_3) (normal) interaction displayed interaction energies nearly in the order 6.0–8.8 kcal mol^{-1} dihalide and 2.5–3.5 kcal mol^{-1} for tetrahalide complexes, respectively. This observation highlights the fact that, beyond the σ-donation from C_{jNHC} to the unfilled Pd d-orbital examined above, there would be a π-backdonation from occupied Pd d-orbitals to the vacant p-orbital of C_{jNHC}. It should, therefore, be noted that the strength of the La[ln]···Pd backbonding is slightly affected by the availability of the lone pairs on the adjacent nitrogen (N_3 or $N_{3'}$) in the imidazole ring (Scheme 1). It is clearly shown from the increasing energy stabilization order **4a** < **3a** < **4n** < **3n** < **2a** < **1a** < **2n** < **1n** observed in all complexes. Three remarkable impacts are observed with the increased stabilization energies: (i) the first one is the nature of halide, (ii) the second one is the chelating model and (iii) the third one is the oxidation state complex. All these trends exhibit greater π-backdonation, which further stabilizes the C···Pd bonds when going from chloride to bromide, normal to abnormal and Pd^{II} to Pd^{IV} complexes, respectively.

3.4.2. Topological analysis. For obtaining a quantitative description of the electronic structure of all complexes, a full topological analysis was carried out based on the theory of atoms in molecules (AIM)[30,31] with special attention to the topological properties of C_{aNHC}···Pdor C_{nNHC}···Pd and Pd···X bond critical points (BCPs). The corresponding topological parameters, such as electron density [$\rho(r)$], its Laplacian [$\nabla^2\rho(r)$], Lagrangian kinetic energy [$G(r)$], potential energy density [$V(r)$], ellipticity (ε), and eta index (η), are listed in Table 4. Independent of the chelating mode of the palladium atom and its oxidation state, the positive values of Laplacian and electron density (less than 0.100 a.u for Pd···X and upper than 0.100 a.u for C_{aNHC}···Pd or C_{nNHC}···Pd interactions) suggest that the latter are closed-shell (ionic) interactions (see Table 4). In addition, these observations confer a weaker and stronger bonding strength for Pd···X and C_{aNHC}···Pd or C_{nNHC}···Pd bonds, respectively, due to the depletion of the density in the interaction region between the atoms. For these bonding interactions, the average values of the electron density ($\rho(r)$) at the BCPs are 0.121 and 0.083 a.u for C_{jNHC}···Pd, 0.054 and 0.046 a.u for Pd···X in different Pd^{II} and Pd^{IV} complexes, respectively. Collectively, we have attributed the great ($\rho(r)$) values observed above for the C_{aNHC}···Pd or C_{nNHC}···Pd bonds for intense to the simultaneous presence of the C_{NHC} → Pd^{i+} strongly σ-donating ligands and the C_{NHC} ← Pd^{i+} π-backbonding due to the existence of d–π* Pd interactions. This double substantial interaction between C_{aNHC}(C_{nNHC}) and Pd atoms plays an important role in the stabilization of the complex. The literature supports this conclusion on the general viability of π-backbonding in metal-NHC complexes.[36] Given the topological properties at the BCPs discussed above, the AIM analysis is in agreement with our NBO previously discussed (see Section 3.4.1). To highlight the quality of data, the featureless residual Laplacian of the total density map is plotted (Fig. 5). When comparing the Laplacian

Table 4 Topological parameters of M···C···metal and M···X ((X= I, Br and Cl)) from B3LYP/GEN data in various binding modes

Mol.	Bond	$\rho(r)$ (a.u)	$\nabla^2\rho(r)$ (a.u)	ELF	$V(\boldsymbol{r})$ (a.u)	$G(r)$ (a.u)	$\frlvert\boldsymbol{V}(\boldsymbol{r})\frrvert/\boldsymbol{G}(\boldsymbol{r})$	$\boldsymbol{H}(\boldsymbol{r})$ (a.u)	E_{int} (kcal mol^{-1})	ε (a.u)
1n	**Pd···C_{NHC}**	0.117	0.475	2.280	−0.182	0.151	1.210	−0.032	−57.133	0.163
	Pd···Cl	0.053	0.233	0.687	−0.069	0.064	1.085	−0.005	−21.648	0.537
2n	**Pd···C_{NHC}**	0.116	0.450	2.271	−0.769	0.145	5.311	−0.032	−241.273	0.129
	Pd···Br	0.051	0.167	0.629	−0.061	0.051	1.183	−0.009	−19.045	0.505
1a	**Pd···C_{NHC}**	0.128	0.302	2.204	−0.183	0.129	1.416	−0.054	−57.385	0.028
	Pd···Cl	0.059	0.183	0.731	−0.065	0.055	1.172	−0.010	−20.300	0.058
2a	**Pd···C_{NHC}**	0.125	0.295	2.197	−0.773	0.126	6.159	−0.052	−242.529	0.031
	Pd···Br	0.054	0.125	0.679	−0.053	0.042	1.255	−0.011	−16.503	0.050
3n	**Pd···C_{NHC}**	0.097	0.441	2.110	−0.148	0.129	1.147	−0.019	−46.435	0.386
	Pd···Cl	0.048	0.232	0.537	−0.063	0.061	1.045	−0.003	−19.829	1.090
	Pd···Cl_{Eq}	0.047	0.219	0.445	−0.061	0.058	1.052	−0.003	−19.045	0.947
	Pd···Cl'_{Eq}	0.047	0.231	0.472	−0.062	0.060	1.033	−0.002	−19.390	0.405
4n	**Pd···C_{NHC}**	0.092	0.340	2.137	−0.138	0.119	1.159	−0.019	−43.235	0.337
	Pd···Br	0.045	0.165	0.536	−0.054	0.048	1.136	−0.007	−17.037	2.313
	Pd···Br^{Eq}	0.044	0.138	0.421	−0.049	0.042	1.173	−0.007	−15.342	1.194
	Pd···Br'^{Eq}	0.043	0.159	0.369	−0.052	0.046	1.131	−0.006	−16.252	1.204
3a	**Pd···C_{NHC}**	0.101	0.491	1.943	−0.169	0.146	1.158	−0.023	−52.961	0.120
	Pd···Cl	0.047	0.217	0.584	−0.061	0.058	1.060	−0.004	−19.264	0.155
	Pd···Cl_{Eq}	0.049	0.223	0.491	−0.063	0.059	1.059	−0.004	−19.641	0.690
	Pd···Cl'_{Eq}	0.046	0.203	0.501	−0.058	0.054	1.068	−0.004	−18.229	0.254
4a	**Pd···C_{NHC}**	0.104	0.452	1.982	−0.160	0.137	1.171	−0.023	−50.169	0.140
	Pd···Br	—	—	—	—	—	—	—		—
	Pd···Br_{Eq}	0.045	0.159	0.434	−0.054	0.047	1.148	−0.007	−16.817	0.871
	Pd···Br'_{Eq}	0.043	0.157	0.436	−0.051	0.045	1.131	−0.006	−16.001	0.313

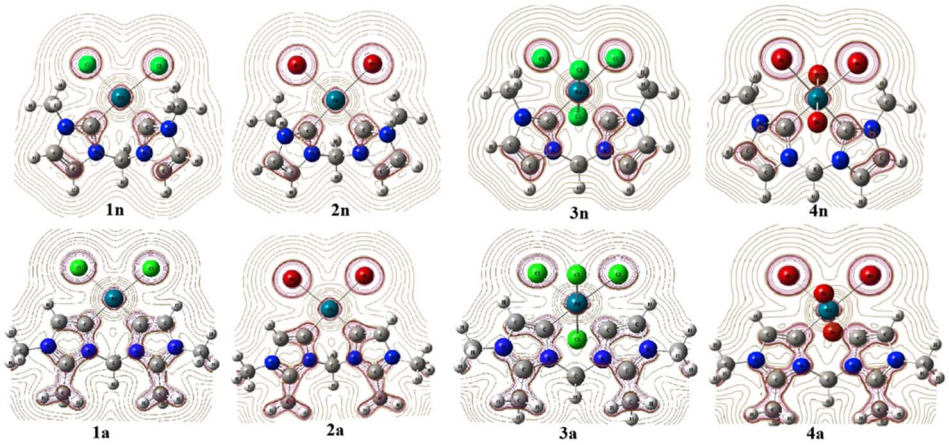

Fig. 5 NPA charges and the Laplacian ($\nabla^2\rho(r)$) of the total density of normal (**1n**, **2n**, **3n**, and **4n**) and abnormal (**1a**, **2a**, **3a**, and **4a**) complexes. Charge concentration regions ($\nabla^2\rho(r) < 0$) are designated with dashed lines.

of the total density of normal and abnormal prototypes of complexes, differences can be seen in the interactions between $C_{aNHC}\cdots Pd$ or $C_{nNHC}\cdots Pd$. The charge concentration part, depicting the lone pair on the C_{aNHC} (in abnormal type) and C_{nNHC} (in normal type) carbons, is responsible for the σ-donor interaction with palladium corresponding to each complex. Collectively, the charge concentration is closer to the C_{aNHC} or C_{nNHC} carbon atom because of the metallic moiety's electron-withdrawing property. In effect, this can be explained by strengthening the $C_{jNHC}\cdots Pd$ bond interaction through σ-donation and π-back donation in abnormal rather than normal complexes, resulting in a denser distribution of electron density. The more compact density distribution is also reflected in the remarkable difference in the NPA charge of C_{jNHC} (Fig. 2S†), which is significantly less negative for the normal complex with the chloride palladium moiety independently of the palladium oxidation state. Additionally, the $Pd^{II}X_2$ and $Pd^{IV}X_4$ moieties also take some electron density from the carbene ligands, decreasing their partial charges. Interestingly, the palladium center becomes slightly more negative in this case (Table 1S†), preserving some of the charge withdrawn from the halide counter-ion. It was observed for the Pd···X interaction, the halide exhibited an unusual behavior by not forming any covalent bond with the Pd atom (Fig. 5), instead remaining isolated with its lone pair and creating a very ionic (closed-shell) interaction. This represents a weaker interaction compared to a covalent or shared-shell interaction and can be considered a halide lone-pair π interaction. Otherwise, the relative closed-shell or lone-pair π interactions of both bond interactions mentioned above may also justify the fact that $C_{aNHC}\cdots Pd$ or $C_{nNHC}\cdots Pd$ and Pd···X interactions are strongly polar, which would lead to a significant accumulation of electron density between the nuclei (C_{NHC}, Pd and X), as in all shared interactions. Thus, the sign of the Laplacian ($\nabla^2\rho(r) < 0$ or $\nabla^2\rho(r) > 0$) in this bond would no longer have an efficient relevance.

Since some covalency is witnessed by $\frac{|V(r)|}{G(r)} > 1$ (the potential energy density $V(r)$ dominates and electrons are stabilized at the BCP),[37] we have integrated this descriptor to obtain further information about the Pd···X and $C_{NHC}\cdots Pd$ interaction at BCP. So, the AIM analysis provides evidence in the series of Pd^{II} and Pd^{IV} complexes, by going from the normal chelating prototype complexes to the abnormal ones, that the Pd···X and $C_{NHC}\cdots Pd$ are partial covalence characters. For example, the covalent character of the Pd···X interaction is strengthened since the average values of $\frac{|V(r)|}{G(r)}$ close successively to 1.134 (**1n** and **2n**), 1.214 (**1a** and **2a**), 1.095 (**3n** and **4n**) and 1.093 (**3a** and **4a**), increase in the following order Pd···Cl < Pd···Br while those of $\nabla^2\rho(r)$ tend to decrease (Table 4). Then, we also integrated with the overall space of bonds, the total energy density ($H(r)$) defined by $H(r) = G(r) + V(r)$ according to Roza criteria[37] and ellipticity (ε) to obtain the ideal behaviour of the electron at BCP. Regardless of chelating model consideration, the negative $H(r)$ values for both interactions (see Table 4) indicate an interaction with significant sharing of electrons. Its magnitude reflects the bond covalency interaction that increases according to the order, C_{NCH}–Pd > Pd–X. Unfortunately, we note the most surprising results unexplained, which come from the **4a** complex for which Table 4 shows the non-existence of BCP in one of $Pd\cdots Br^{eq}$. Focusing on the ellipticity that depends on the instability of the bond, it has the property of determining the presence of a π-like character of the bonding up to the limit of the double bond for which the ellipticity reaches a maximum.[38] Table 4 also shows that, regardless of Pd in its oxidation states (+2 and +4) and bis(jNHC) type complexes consideration, the ellipticity's collective positive values range from 0.1202 to 2.3131 a.u in C_{jNCH}–*Pd* and from 0.3127 to 1.1943 a.u. in Pd–X bonding interactions. Such values well above zero highlighted a formal double bond and exhibited higher instability of these interactions.[39] Although these values reflect a large perturbation from an ideal double bond, they are significantly greater than other corresponding values reported for **1a** and **2a** abnormal complexes in which values of ellipticity obtained, ranging from 0.028 to 0.058 a.u for C_{aNCH}–Pd and Pd–X bonds, close to 0.0 a.u (see, Table 4) indicated a cylindrically symmetrical (simple

bond) form.[38] Therefore, the ellipticity data do not clearly corroborate with the results of the analyses. This could possibly be due to the highly polarised nature of the σ-bonding previously mentioned.

We have again evaluated the strengths of these bonds by using instantaneous interaction energy (E_{int}) defined by the formula $E_{int} = \frac{V(r)}{2}$ at BCPs according to Espinosa–Molins–Lecomte criteria. The calculated values have been gathered in Table 4. Higher E_{int} values (241.3 and 242.5 kcal mol^{-1}) exhibited by **2n** and **2a** (bromide complexes), respectively, in the Pd^{II} type indicate stronger C_{jNCH}–Pd interaction. The reverse fact is observed in Pd^{IV} type complexes for which the E_{int} of C_{jNCH}–Pd in **3n** (46.4 kcal mol^{-1}) and **3a** (53.0 kcal mol^{-1}) chloride complexes are strengthened (Table 4). Such observations suggest a preferential catalytic activity of chloride complexes in the high Pd oxidation state over bromide complexes and reciprocally, based on the strength of the ligand···palladium interaction. These probably justified the choice of high Pd oxidation state (+4) for chloride complexes by Scott McCall[24] and low Pd oxidation state (+2) for bromide complexes by Munz[40] as catalyst for direct C–H bond functionalization reactions respectively of alkenes, alkynes, and alkanes. For the Pd–X bonds, the E_{int} values ranging from 15.3 to 21.6 kcal mol^{-1} fall within the range of typical halogen-bond energies (2.4–47.9 kcal mol^{-1}),[41] which indicated weak bond interaction forms. In addition, Table 4 also shows that the quantity E_{int} is inversely proportional to the size of the halide (Cl < Br) in each chelation mode of complexes independent of the Pd oxidation state form adopted. In the end, at this stage, the interpretation of the AIM data of these bonds is delicate since they describe an intermediate situation.

For a better prediction of the chemical bond properties of all complexes, we combined the AIM study with ELF population analysis. Fig. 6 and 4S† show the presence of ELF basin attractor on C_{jNHC}–Pd and Pd–X at BCPs, meaning that the electrons are shared by the two elements involved. According to the well-known ELF basin symbolic method, the presence of these basins should be identified as V(C_{jNHC},Pd) and V(Pd,X). Table 4 depicts some integrals, namely the average electron population number in each basin. The result shows that the average integral of electron density in V(Pd, X) and V(C_{jCNH}, Pd) are 1.0 and 2.1e, respectively. Evidently, the bonding between C_{NHC}–Pd is much stronger than Pd – X; this is why the bond length of the former (close to 2.0 Å) is shorter than the latter (close to 2.5 Å). Note that the greater electron population number in V(C_{jNHC}, Pd) of Pd^{II} compared to Pd^{IV} prototype complexes are 2.28 (**1n**), 2.27(**2n**), 2.20 (**1a**) and 2.20 (**2a**) (Table 4); therefore, it can be expected generally that $C_{carbene}$–Pd bonds of dihalide complexes are stronger than tetrahalides ones. The ELF population number in V(C_{jCNH}, Pd) and V(Pd, X) approximately reflecting that there is a pair of electrons shared between C_{jCNH} and Pd and an ionic bond interaction between Pd and X.

To measure both C_{jCNH}–Pd and Pd–X bond strengths, which represent the combined covalent and ionic bond, Wiberg (WI) and Mayer (MI) bond orders are reported to be very well correlated with their description. Note that the Mayer bond order can be seen as a generalization of the Wiberg bond order for a restricted close-shell system.[42] In our study, the WI and MI of both bonds on all the complexes were computed. The WI and MI values in Fig. 7 indicate that all the Pd^{IV} complexes present a C_{jCNH}–Pd bond order (1.118–1.250 for WI and 1.127–1.255 for MI) greater than 1.0 a.u compared with those for all Pd^{II} complexes (0.750–0.784 for WI and for 0.897–0.914 for MI) and less than 1.0 a.u indicated that the former are stronger covalent bonds. The reverse fact is observed for the Pd–X bond order for which greater WI values close to 1.1 for Pd^{II} complexes could exhibited a slightly covalent bond compared with Pd^{IV} complexes (close to 0.89) (see Fig. 7b). From this previous Figure, although the WI values slightly increase from Pd^{IV} to Pd^{II} complexes, they are significantly greater than the MI values reported for Pd–X bonds in all complexes, which range from 0.45 to 0.75. These observations mainly suggest the marginally larger *trans* influence of bromide *vs.* chloride and confirmed by geometrical analysis (see Section 3.1).

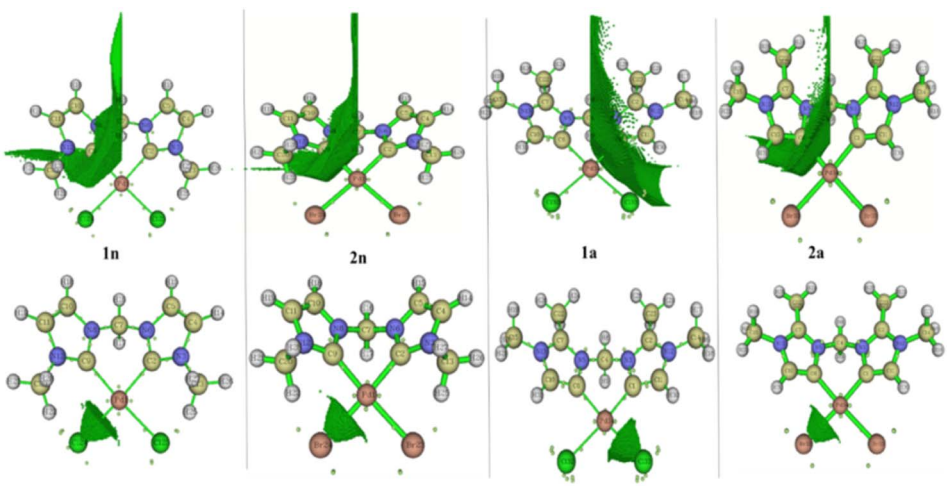

Fig. 6 Local region basin one C_{jNHC}–Pd and Pd–X in **1n**, **1a**, **2n** and **2a** complexes.

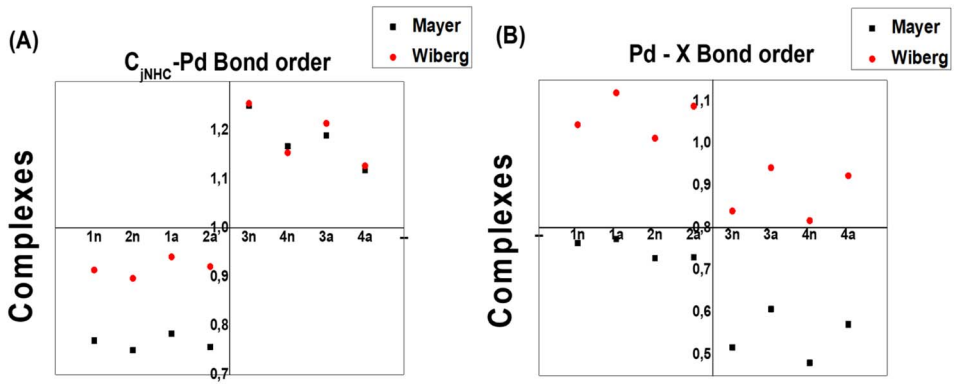

Fig. 7 Wiberg and Meyer bond index values of C_{jNHC}–Pd and Pd–X for complex structures.

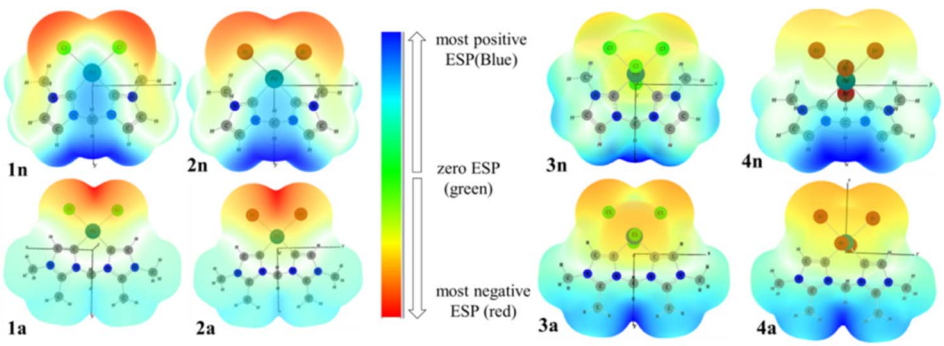

Fig. 8 3D MEP surfaces of Pd^{II} (**1n**, **2n**, **1a** and **2a**) and Pd^{IV} (**3n**, **4n**, **3a** and **3a**) complexes, mapped onto electron density isosurfaces of value 0.02 a.u., using GaussView.

3.5. Molecular electrostatic potential (MEP) surfaces

To investigate the reactive sites for electrophilic and nucleophilic attacks, the MEP surfaces for Pd^{II} and Pd^{IV} complexes have been plotted (Fig. 8). MEP surface is an electron density isosurface from SCF density mapped with an electrostatic potential surface (ESP). It is used to determine their sizes, shapes, and reactive sites on complexes in the case of eventual catalytic reactions. According to the literature, negative (red and yellow) and positive (light and dark blue) regions of the MEP surfaces are related to electrophilic and nucleophilic reactivity, respectively, while the green or white region corresponds to the limitation between negative and positive regions (zero electrostatic potential). The obtained results from MEP are mapped in Fig. 8(A), which shows that the red region of the MEP surface for Pd^{II} complexes is mainly localized over the different halide atoms, suggesting the most suitable atomic sites for a possible electrophilic attack. Moreover, in **1n** and **2n** complexes, the maximum blue region is localized on the C_{nNHC}–Pd, and N_3–C bonds that form the pallado-cycle and C–H of the CH_2 bridged, showing that they are possible sites for attack by nucleophiles heavily weighted on CH_2 methylene bridged. From the MEP maps in Fig. 8(B), it is also clear that the regions of **3n**, **4n**, **3a** and **4a** with the most negative $V(r)$ are associated with the all-chloride ions. Hence, the most favourable atomic site for the electrophilic attack on these complexes is the PdX_4 metallic moiety.

4 Conclusion

Although several existing bis(NHC) palladium complexes have been reported to have successful catalytic efficiency in C–H bond activation, their intrinsic binding properties on the efficacy of catalytic activity are currently under increasing investigation. This has motivated an urgent search to understand the factors underlying this catalytic activity. In this regard, the present work has used Density Functional Theory calculations to elucidate more about the nature of C_{aCNH}–Pdor C_{nCNH}–Pd and Pd–X (X= Cl or Br) bond interactions, which have been found to play a key role based on the design criteria. The results of this work have conclusively demonstrated that thermodynamically favourable interactions can exist between bis(aNHC) or bis(nNHC) and Cl or Br halide ions with Pd^{II} and Pd^{IV} oxidation state, respectively, for the complex formation process. The calculated results show that both bis(aNHC) or bis(nNHC) ligands and the coordinating halides influence the strength of the C_{aCNH}–Pdor C_{nCNH}–Pd bonds. NBO methods clearly reveal the extent of σ-donation and π-backdonation for these bonds and help to understand the tunability of the complex structures. The σ-donation and π-backdonation are highest in the chlorine complexes and lowest in the bromine complexes. In addition, AIM analysis revealed that the greater covalent nature and strength of the C_{jNHC}–Pd bond than Pd–X bonds depend on the

nature of the oxidation state of palladium as well as the coordinating halide ion. The geometric aspect reveals the presence of C_{2v} pseudo-symmetry and suggests that bromide is the weakly coordinating ligand compared to chlorides. Overall, the results show that bis(aNHC) and bis(nNHC) ligands appeared to be a suitable choice as ancillary support for Pd^{IV} due to their known propensity to stabilize highly oxidized metal centers without ligand dissociation. Thus, the resulting complexes can be made better catalyst precursors with preferred normal or abnormal coordination mode ligands on palladium and choosing a weakly coordinating halide.

Data availability

Data will be made available on request.

Conflicts of interest

The authors declare that they have no known competing financial interests or personal relationships that could have appeared to influence the results reported in this paper.

Acknowledgements

This work was supported by the Ministry of Higher Education of Cameroon. The calculations were performed on the computers of the Consortium des Equipments de Calcul Intensif (CECI, http://www.ceci-hpc.be) and particularly those of the Technological Platform of High-Performance Computing, for which the authors gratefully acknowledge the financial support of the FNRS-FRFC, of the Walloon Region, and of the University of Namur (Conventions No. 2.5020.11, GEQ U.G006.15, 1610468, and RW/GEQ2016).

References

1 «Le pétrole n'est pas renouvelable», 2020https://www.connaissancedesenergies.org/le-petrole-nestpas-renouvelable150513#notes. Accessed August 26.
2 BP, *BP Statistical Review of World Energy 2016*, 2016.
3 https://gazissimo.fr/conseils/conso-energie.
4 B. L. Conley, W. J. Tenn III, K. J. H. Young, S. K. Ganesh, S. K. Meier, J. Oxgaard, J. Gonzales, W. A. Gaddard III and R. A. Periana, *Activation of Small Molecules: Organometallic and Bioinorganic Perspectives*, Wiley-VCH, Weinheim, 2006, p. 235.
5 A. E. Shilov and G. B. Shulpin, *Chem. Rev.*, 1997, **97**, 2879.
6 N. F. Goldshleger, V. V. Eskova, A. E. Shilov and A. A. Shteinman, *Zh. Fiz. Khim.*, 1972, **46**, 1353.
7 A. J. Arduengo, R. L. Harlow and M. Kline, *J. Am. Chem. Soc.*, 1991, **113**, 361.
8 L. Mercsa and M. Albrecht, *Chem. Soc. Rev.*, 2010, **39**, 1903.
9 H. Jacobsen, A. Correa, A. Poater, C. Costabile and L. Cavallo, *Coord. Chem. Rev.*, 2009, **253**, 687.
10 D. Munz and T. Strassner, *Angew. Chem., Int. Ed.*, 2014, **53**, 2485.
11 D. Munz, D. Meyer and T. Strassner, *Organometallics*, 2013, **32**, 3469.
12 W. A. Herrmann, J. Schwarz and M. G. Gardiner, *Organometallics*, 1999, **18**, 4082.
13 J.-Q. Liu, X.-X. Gou and Y.-F. Han, *Chem.–Asian J.*, 2018, **13**, 2257.
14 J. A. Mata, M. Poyatos and E. Peris, *Coord. Chem. Rev.*, 2007, **251**, 841.
15 X. Hu and K. Meyer, *J. Organomet. Chem.*, 2005, **690**, 5474.
16 M. G. Gardiner and C. C. Ho, *Coord. Chem. Rev.*, 2018, **375**, 373.
17 T. Yagyu, A. Tsubouchi and Y. Nishimura, *J. Organomet. Chem.*, 2014, **767**, 1.
18 (*a*) A. Krüger and M. Albrecht, *Aust. J. Chem.*, 2011, **64**, 1113; (*b*) G. Guisado-Barrios, J. Bouffard, B. Donnadieu and G. Bertrand, *Angew. Chem., Int. Ed.*, 2010, **49**, 4759.
19 V. Khlebnikov, M. Heckenroth, H. Müller-Bunz and M. Albrecht, *Dalton Trans.*, 2013, **42**, 4197.
20 M. Heckenroth, E. Kluser, A. Neels and M. Albrecht, *Dalton Trans.*, 2008, **44**, 6242.
21 T. Strassner, M. Muehlhofer, A. Zeller, E. Herdtweck and W. A. Herrmann, *J. Organomet. Chem.*, 2004, **689**, 1418.
22 R. Jagadeesan, G. Velmurugan and P. Venuvanalingam, *RSC Adv.*, 2015, **5**, 80661.
23 J. M. Ongagna, A. D. T. Fouegue, B. A. Ateba, G. D. Mouzong, J. Z. Mfomo, L. M. Mbaze and D. M. Bikele, *J. Mol. Model.*, 2020, **246**, 9.
24 A. S. McCall, H. Wang, J. M. Desper and S. Kraft, *J. Am. Chem. Soc.*, 2011, **133**, 1832.
25 M. Frisch, G. W. Trucks, H. B. Schlegel, G. E. Scuseria, M. A. Robb, J. R. Cheeseman, G. Scalmani, V. Barone, B. Mennucci, G. A. Petersson, *et al.*, *Gaussian 16, Revision A. 03*, Gaussian Inc., Wallingford, CT, 2016.
26 T. Lu and F. Chen, *J. Comput. Chem.*, 2012, **33**, 580–592.
27 P. Geerlings, F. De Proft and W. Langenaeker, *Chem. Rev.*, 2003, **103**, 1793.
28 R. Shankar, K. Senthilkumar and P. Kolandaivel, *Int. J. Quantum Chem.*, 2009, **109**, 764.
29 J. Martínez, Local reactivity descriptors from degenerate frontier molecular orbitals, *Chem. Phys. Lett.*, 2009, **478**, 310–322.
30 R. Chauvin, C. Lepetit, B. Silvi and E. Alikhani, *"Applications of Topological Methods in Molecular Chemistry*, Springer, Berlin. 2016.
31 R. F. W. Bader, *Chem. Rev.*, 1991, **91**, 893.
32 D. Cremer and E. Kraka, *Angew Chem. Int. Ed. Engl.*, 1984, **23**, 627.
33 F. Weinhold and C. R. Landis, *Chem. Educ. Res. Pract.*, 2001, **2**, 91.
34 L. R. Domingo, M. J. Aurell, P. Perez and R. Contreras, *Tetrahedron*, 2002, **58**, 4417.
35 S. I. Gorelsky, S. Ghosh and E. I. Solomon, Mechanism of N2O Reduction by the μ4-S Tetranuclear CuZCluster of Nitrous Oxide Reductase, *J. Am. Chem. Soc.*, 2006, **128**, 278–290.
36 J. Haller, N. Kaltsoyannis, M. J. Sarsfield, I. May, S. Cornet, M. Redmond and M. Helliwell, *Inorg. Chem.*, 2007, **46**, 4868.

37 D. Cremer and E. Kraka, *Angew Chem. Int. Ed. Engl.*, 1984, **23**, 627.
38 *The Quantum Theory of Atoms in Molecules*, ed. Che'rif F. Matta and J. Boyd Russell, WILEY-VCH Verlag GmbH & Co. KGaA, Weinheim, 2007, Copyright 8, ISBN: 978-3-527-30748-7.
39 M. K. Samantaray, D. Roy, A. Patra, M. Saikh, R. B. Sunoj and P. Ghosh, *J. Organomet. Chem.*, 2006, **691**, 3797.
40 D. Munz and T. Strassner, *Top. Catal.*, 2014, **57**, 1372.
41 P. Metrangolo, F. Meyer, T. Pilati, G. Resnati and G. Terraneo, *Angew. Chem.*, 2008, **47**, 6114.
42 W. Su, S. Pan, X. Sun, S. Wang, L. Zhao, G. Frenking and C. Zhu, *Nat. Commun.*, 2018, **9**, 4997.